Passages de Paris 1 (2005) 238–250

www.apebfr.org/passagesdeparis

VIBRATIONS OF THICK PLATES USING LAGRANGEAN QUADRILATERAL FINITE ELEMENT WITH 16 NODES*

Marcus V. Girão DE MORAIS**
Lineu J. PEDROSO
Selenio F. DA SILVA

Abstract: This paper presents a study on the dynamic behaviour of thick plates on free vibrations. The Reissner theory is applied to model the plate which is discretized using the Finite Elements Method employing a sixteen-node Bicubic Lagrangian Element. With a view on testing the element's potential, several boundary conditions, plate shapes and thickness ratios were simulated. Whenever it was possible, the results obtained were compared to analytical and experimental solutions.

Key words: Dynamic of plates; Thick plates; Reissner-Mindlin theory; Finite Elements Method; Bicubic Lagrangian Element.

Resumo: Esse artigo apresenta um estudo sobre o comportamento dinâmico de placas finas em vibração livre. A teoria Reissner é aplicada na modelização da placa discretizada através do Método dos Elementos Finitos utilizando um elemento Bicúbico Lagrangiano com 16 nós. Várias condições de contorno, formas e espessuras de placas foram simuladas a fim de testar o potencial desse tipo de elemento. Sempre que possível, os resultados foram comparados a soluções analíticas e a resultados experimentais.

Palavras-chave: Dinâmica de placas; Placas finas; Teoria de Reissner-Mindlin; Método de Elementos Finitos; elemento Bicúbico Lagrangiano.

I. INTRODUCTION

The "plate state" principle is applied on design of several engineering structures, such as bridge boards, tracking systems, retaining walls, water tanks, ships' hulls, car parts, spacecrafts and nuclear reactors.

Basically, the plate theories vary according to the hypotheses regarding the rotation of normal direction on the middle surface. Hence the classical theory of Kirchhoff thin plates determines that these normal directions remain straight and orthogonal when the plate is bent [1,2]. Theories such as the Reissner-Mindlin, however, conserve the

* Revised version of "Vibração livre de Placas de Reissner-Mindlin pelo Método dos Elementos Finitos" published originally in 20th iberian latin-american congress on computacional methods in enginnering records.

** Marcus V. GIRÃO DE MORAIS - ATER IUP Génie Civil - Université de Cergy-Pontoise (UCP) - UFR Sciences et Techniques - IUP Génie Civil et Infrastructures. E-mail: mumorais@hotmail.fr

straight strain state of the normal direction, but do not require it to be orthogonal with the strain of the middle surface [3,4].

The plate elements based on Kirchhoff theory are used only on thin plates (thickness/width ≤ 0.10) and they have many difficulties to find shape functions that meet the requirements of deflection continuity in element. An alternative formulation, which is based on theory of Reissner-Mindlin plates, can be applied to thin and thick plates and it also helps eliminate the difficulties regarding Kirchhoff elements. Further details on the plate and finite elements theories developed for plate bending can be found, for instance, in [5,6,7,8]. This paper analyses the dynamic behaviour on free vibrations of rectangular and circular plates based on Reissner-Mindlin theory. The sixteen-node Lagrangian quadrangle (QL16) is used as a plate finite element, in the scope of a research program [9].

II. THEORICAL FUNDAMENTALS

The displacement field $\bar{u}$, deflections $\varepsilon^{(e)}$ e strains $\sigma^{(e)}$ of an element can be expressed as follows:

$$\bar{\mathbf{u}}(x,y,z,t)=[\Phi(x,y,z)]u^{(e)}(t), \quad \varepsilon^{(e)} = \mathbf{B}\mathbf{u}^{(e)} \quad \text{and} \quad \sigma^{(e)} = \mathbf{D}\mathbf{B}\mathbf{u}^{(e)} \tag{1}$$

where, Φ represents the shape functions matrix and $\mathbf{u}^{(e)}$ is the nodal displacement vector of the element, which is taken as function of time t. By applying the Hamilton Principle in order to obtain the dynamic equation of the structure, we arrive at,

$$d\{\partial L/\partial \dot{u}\}/dt - \{\partial L/\partial u\} = \vec{0} \tag{2}$$

where, the Lagrangian element is defined as: $L = C-\Pi_p$; C represent the kinetic energy and Π_P is the potential energy, $\mathbf{u}$ is the nodal displacement vector and $\dot{u}$ is the global nodal velocity of the structure. The kinetic and potential energies can be written as,

$$\begin{cases} C^{(e)} = \dfrac{1}{2}\iiint_{V^{(e)}} \rho \dot{\mathbf{u}}^{(e)^T} \dot{\mathbf{u}}^{(e)} dV \\ \Pi_P^{(e)} = \dfrac{1}{2}\iiint_{V^{(e)}} \varepsilon^{(e),T} \sigma^{(e)} dV \end{cases} \tag{3}$$

where, $V^{(e)}$ is element volume, ρ is mass density, $\dot{u}^{(e)}$ is velocity vector of an element (e). Using expressions from Equation 1, the terms in C and Π_p of an element can be expressed as,

$$\begin{cases} C = \sum_{e=1}^{E} C^{(e)} = \frac{1}{2}\dot{u}^T \left[\sum_{e=1}^{E} \iiint_{V^{(e)}} \rho[\Phi]^T[\Phi]dV \right] \dot{u} \\ \Pi_P = \sum_{e=1}^{E} \Pi_P^{(e)} = \frac{1}{2} u^T \left[\sum_{e=1}^{E} \iiint_{V^{(e)}} [\mathbf{B}]^T[\mathbf{D}][\mathbf{B}]dV \right] u \end{cases} \quad (4)$$

The stiffness and mass matrixes of an element are now defined through integrals as follows,

$$[M^{(e)}] = \iiint_{V^{(e)}} \rho[\Phi]^T[\Phi]dV \quad \text{and} \quad [K^{(e)}] = \iiint_{V^{(e)}} [B]^T[D][B]dV \quad (5)$$

From Equation 5, the terms of Equation 4 can be rewritten: $C = \frac{1}{2}\dot{\mathbf{u}}^{(e),T}[M]\dot{\mathbf{u}}^{(e)}$ and $\Pi_p = \frac{1}{2}u^{(e),T}[K]u^{(e)}$, and also the global mass and stiffness matrixes $[\mathbf{M}] = \Sigma[M^{(e)}]$ and $[\mathbf{K}] = \Sigma[K^{(e)}]$, which can be replaced in Equation 2, in order to obtain the dynamic balance equation of the structure. Considering harmonical displacements of the type $u(t) = \Lambda_n e^{i\omega nt}$, the equation of free vibrations is obtained:

$$\left\{[K] - \omega_n^2[M]\right\}\Lambda_n = 0 \quad (6)$$

III. REISSNER-MINDLIN PLATES

The kinematic assumptions on the theory of Reissner plates [3] relate displacements (U,V,W) of a generic point in the plate to displacements (u,v,w) rotations (θ_x, θ_y) in its middle surface through:

$$U(x,y,z) = u(x,y) - z\theta_y(x,y);\ V(x,y,z) = v(x,y) - z\theta_x(x,y);\ W(x,y,z) = w(x,y) \quad (7)$$

where z is normal direction on middle plan. Based on Reissner-Mindlin hypothesis regarding the non-perpendicularity of the normal directions on middle surface, we obtain the following:

$$\theta_x = (\partial w/\partial x) + \phi_x \ \text{ e } \ \theta_y = (\partial w/\partial y) + \phi_y \quad (8)$$

where $\partial w/\partial x$ and $\partial w/\partial y$ represent the rotations of normal direction in a given point due to a change in inclination of middle surface and ϕ_x and ϕ_y correspond to the additional rotation of normal direction, not necessarily in an orthogonal position regarding the middle surface strain. The additional rotations are deflections caused by transversal shearing γ_{xz} and γ_{yz}.

The stress and strain state are described through five generalised quantities,

$$\sigma^T = [\sigma_f, \sigma_c] \ \text{ e } \ \varepsilon^t = [\varepsilon_f, \varepsilon_c] \quad (9)$$

where $\sigma_f^T = [M_x , M_y , M_{xy}]$ and $\sigma_c^T = [Q_{xz} , Q_{yz}]$ correspond, respectively, to the stress vectors due to bending effects (M_x , M_y , M_{xy}) and shearing (Q_{xz} , Q_{yz}); while $\varepsilon_f^T = [\kappa_x , \kappa_y , \kappa_{xy}]$ and $\varepsilon_c^T = [\theta_{xz} , \theta_{yz}]$ also correspond to strain vectors due to bending and shearing effects; κ_x , κ_y and κ_{xy} are quantities related to curvatures in x and y and torcional curvatures in xy, and $\theta_{xz} , \theta_{yz}$ represent the rotations regarding the xz and yz plans. The shearing quantities are expressed by $Q_{\alpha z} = \chi G t \gamma_{\alpha z}$, where χ is an shearing correction factor.

IV. FINITE ELEMENT DISCRETIZATION

As deflection and rotations are dependent variables, each term can be separately interpolated in displacement vector using same shape functions for QL16 element for each case (Figure 1).

$$u = \{ w \quad \theta_x \quad \theta_y \}^T = \sum_{i=1}^{16} \{ \phi_i w_i \quad \phi_i \theta_{x\,i} \quad \phi_i \theta_{y_i} \}^T \tag{10}$$

where ϕ_i represent the shape functions and w_i , $\theta_{y,i}$ or $\theta_{x,i}$ are nodal displacements or rotations. Equation 10 expresses displacement field u for each node, with an interpolation of functions ϕ_i.

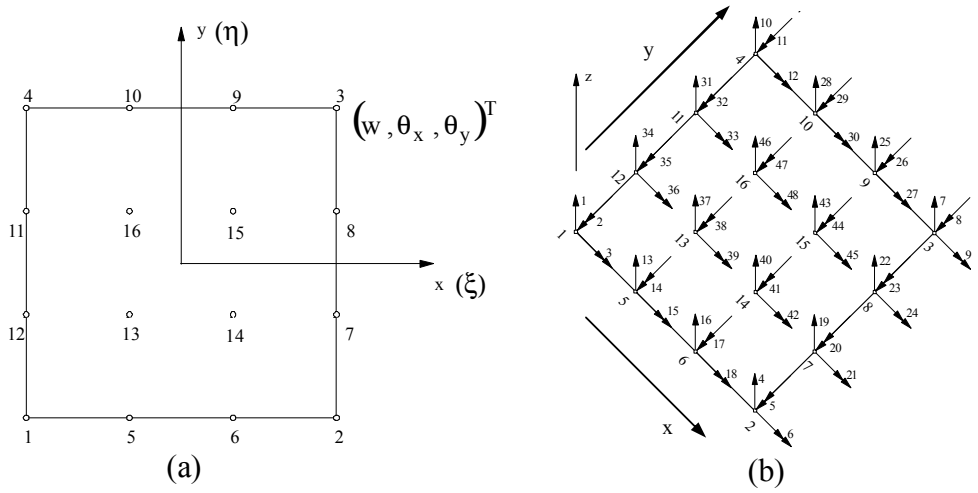

Figure 1 - Plate Finite Element QL16 (a);
Distribution of QL16 Element Displacements (b).

Hence the generalised strain vector can be expressed by Equation 9 as:

$$\varepsilon_f = \sum_{i=1}^{16} \left\{ -\frac{\partial \phi_i}{\partial x}\theta_{x,i} \quad -\frac{\partial \phi_i}{\partial y}\theta_{y,i} \quad -\left(\frac{\partial \phi_i}{\partial y}\theta_{x,i} + \frac{\partial \phi_i}{\partial x}\theta_{y,i} \right) \right\} = \sum_{i=1}^{16} B_{f,i}\, u_i^{(e)}$$
$$\varepsilon_c = \sum_{i=1}^{16} \left\{ \frac{\partial \phi_i}{\partial x} w_i - \phi_i \theta_{x,i} \quad \frac{\partial \phi_i}{\partial y} w_i - \phi_i \theta_{y,i} \right\} = \sum_{i=1}^{16} B_{c,i}\, u_i^{(e)} \tag{11}$$

The generalised strain matrix **B** of an element is obtained, and $\mathbf{B} = \{\mathbf{B}_f\ \mathbf{B}_c\}$, where $\mathbf{B}_f$ and $\mathbf{B}_c$ are bending and transversal shearing generalised strain matrixes of an element. The plate stiffness matrix is obtained from Equations 5 and 11 through the analysis of $\mathbf{B}^T\,\mathbf{D}\,\mathbf{B}$.

$$B^T DB = \begin{Bmatrix} 0 & 0 & 0 & \frac{\partial \phi_i}{\partial x} & \frac{\partial \phi_i}{\partial y} \\ -\frac{\partial \phi_i}{\partial x} & 0 & -\frac{\partial \phi_i}{\partial y} & -\phi_i & 0 \\ 0 & -\frac{\partial \phi_i}{\partial y} & -\frac{\partial \phi_i}{\partial x} & 0 & -\phi_i \end{Bmatrix} \begin{Bmatrix} \overline{D}_f & \nu\overline{D}_f & 0 & 0 & 0 \\ \nu\overline{D}_f & \overline{D}_f & 0 & 0 & 0 \\ 0 & 0 & M\overline{D}_f & 0 & 0 \\ 0 & 0 & 0 & \overline{D}_c & 0 \\ 0 & 0 & 0 & 0 & \overline{D}_c \end{Bmatrix} \begin{Bmatrix} 0 & 0 & 0 & \frac{\partial \phi_i}{\partial x} & \frac{\partial \phi_i}{\partial y} \\ -\frac{\partial \phi_i}{\partial x} & 0 & -\frac{\partial \phi_i}{\partial y} & -\phi_i & 0 \\ 0 & -\frac{\partial \phi_i}{\partial y} & -\frac{\partial \phi_i}{\partial x} & 0 & -\phi_i \end{Bmatrix}^T \tag{12}$$

Considering that $\overline{D}_c = 5hE/\{12(1+\nu)\}$, $\overline{D}_f = Eh^3/\{12(1+\nu)$ and $M = (1-\nu)/2$, where ν = Poisson coefficient, E = elasticity modulus of the material, $\overline{D}_f$ = plate bending stiffness, $\overline{D}_c$ = plate shearing stiffness, ϕ_i and $\partial\phi_i/\partial x$ (or $\partial\phi_i/\partial y$) are shape functions of QL16 element, and its derivatives in x and y.

Considering an isotropic material (ρ = constant) and applying an adequate Jacobian for the case, we can obtain, the translational and rotational terms of elementary mass matrix respectively as:

$$m_{ij} = \rho \frac{A\,h}{4} \int_{-1}^{+1}\int_{-1}^{+1} \phi_i\, \phi_j\, d\eta\, d\xi \quad \text{and} \quad m_{ij} = \rho \frac{A\,h^3}{48} \int_{-1}^{+1}\int_{-1}^{+1} \phi_i\, \phi_j\, d\eta\, d\xi \tag{13}$$

Hence, the consistent mass matrix of QL16 element has a 48x48 order.

V. NUMERICAL EXAMPLES

The results have been compared to analytical solutions of the Kirchhoff model [2,10], to analytical solutions of the Dawe and Roufaeil models [11], to experimental results and/or to results obtained through the DKQ element of SAP90 [12].

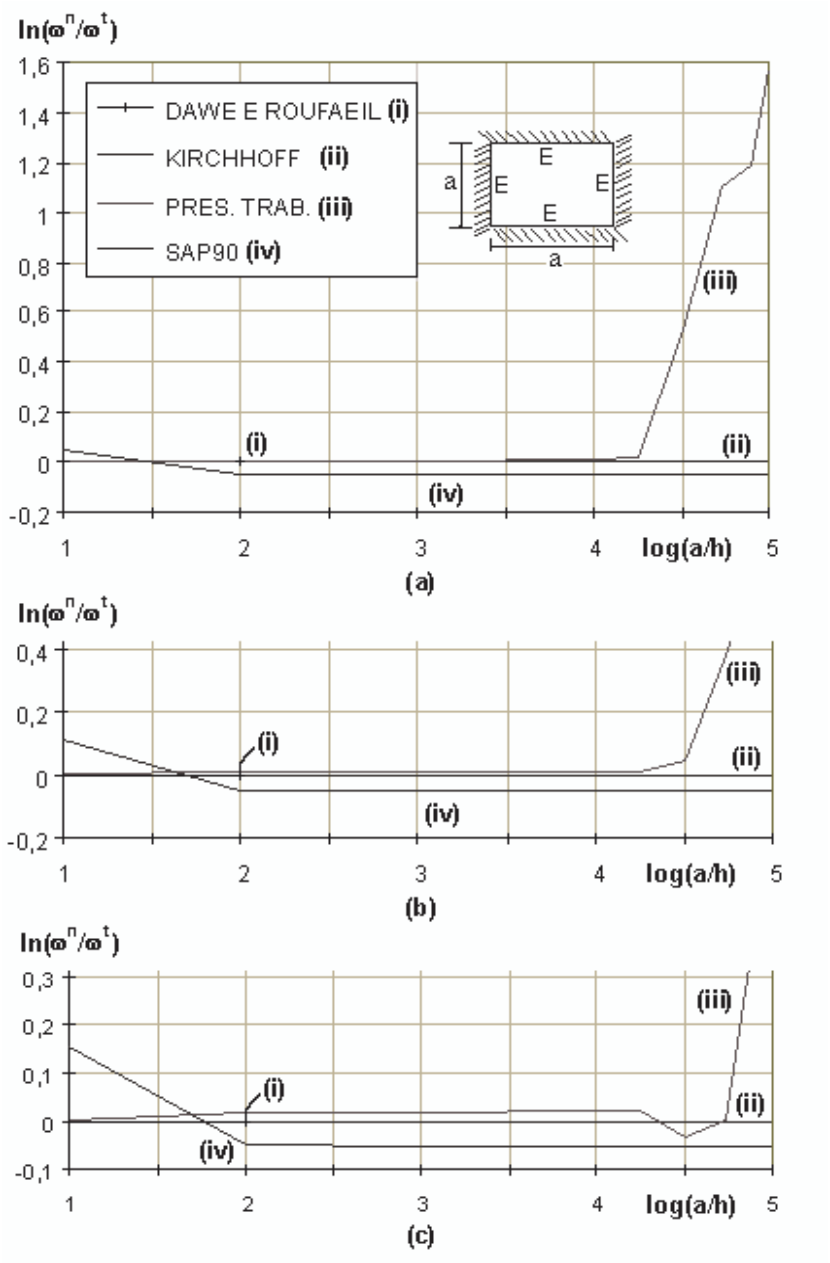

Figure 2 - Representation of *Shear Looking* to element QL16: (a) 1°, (b) 2° e (c) 3° frequencies.

V. 1. Example 1 - Slenderness Limit of Element QL16

In this example, the slenderness limit of the QL16 element is studied by decreasing the slenderness of the plate until there is a solution blocking. A fully clamped square plate (a *x* a) with h thickness is employed. Discretization in *3x3* elements is sufficient in this case [9]. This table also displays the values of the classical solution of Leissa [10], of

the comparative solution of Dawe & Roufaeil [11] and of the Shell (DKQ) element from program SAP90 [12] (Figure 2).

V. 2. Example 2

Analytical, experimental and numerical results regarding a rectangular metallic plate with dimensions a *x* b *x* h and suspended by two strings are compared (Figure 3).

The case presents the following values: $E = 2.00x10^{11} N/m^2$, $\rho = 7800\ kg/m^3$, $\nu = 0.30$, and h = 3/8" (9.525mm).

V. 2 .1. Theorical Results

The analytical values for totally free plates are [2,10]:

$$f_{mn} = \lambda_{mn}/(2\pi a^2)\cdot(D/\overline{m})^{1/2}$$

where $D = Eh^3/[12(1-\nu^2)]$ represents the plate stiffness and $\overline{m} = \rho h$, f_{mn} = frequency in hertz and λ_{mn} is the frequency value. Hence the frequency sequence is obtained:

f_{22} = 533 Hz	f_{13} = 1361 Hz	f_{31} = 686 Hz
f_{32} = 1456 Hz	f_{23} = 1089 Hz	f_{41} = 2138 Hz

V. 2. 2. Experimental Results

The experimental frequency values obtained are as follows [13]:

f_{22} = 543.11Hz	f_{13} = 726.11Hz	f_{31} = 1040Hz
f_{32} = 1310Hz	f_{23} = 1470Hz	f_{41} = 2050Hz
f_{34} = 2490Hz	f_{33} = 2550Hz	

V. 2. 3. Numerical Results

A 3x3 QL16-element mesh has been used to discretize the plate. The numerical and experimental results are coincident for the eight modal vibration shapes analysed [9].

Figure 4 shows the curves referring to experimental, analytical, and numerical results. The results have obtained a satisfactory accordance.

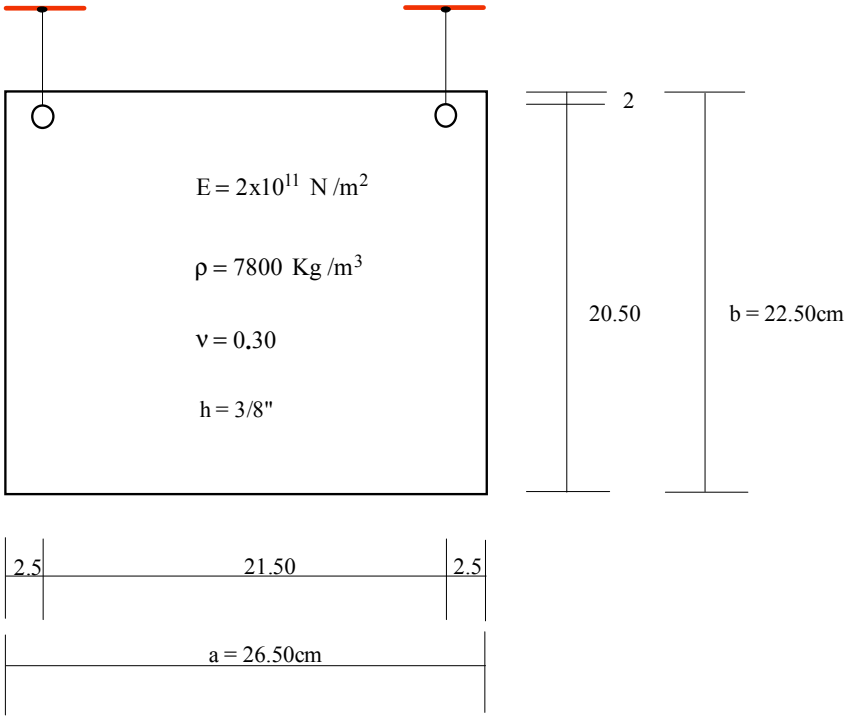

(a)

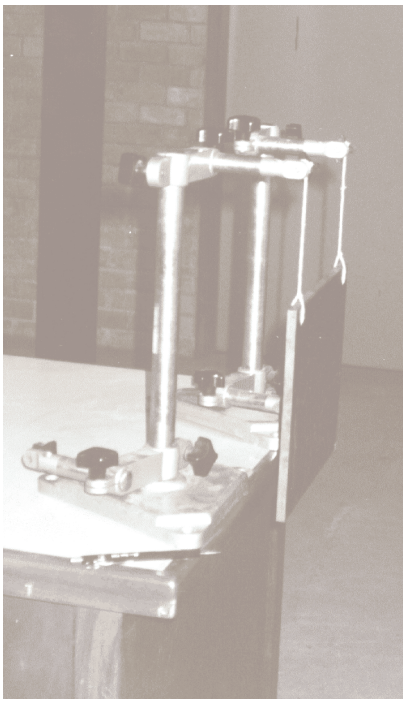

(b)

Figure 3 - Experimental Scheme of Tested Plate (a) and Lateral View (b).

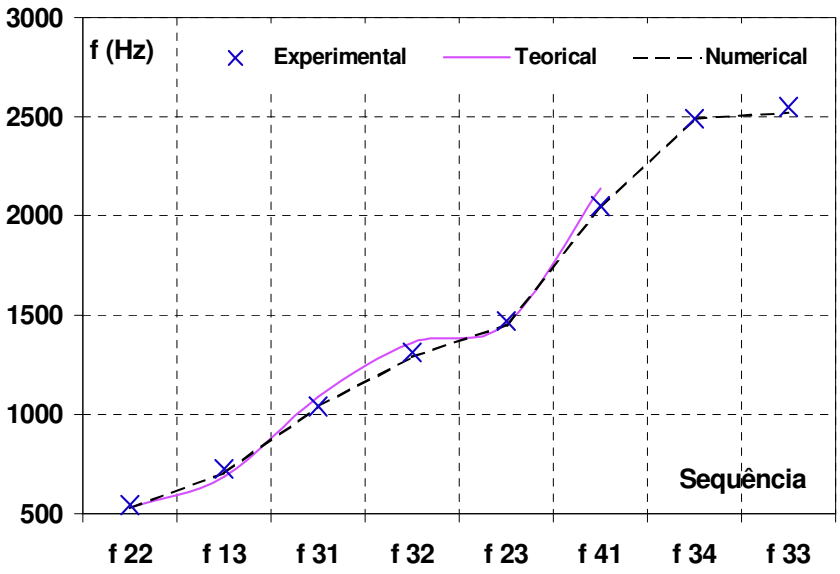

Figure 4 - Representation of Experimental, Numerical and Theoretical Frequency Graphics.

V. 3. Example 3

A circular plate with $r_o = 6.0$m and thickness $h = 0.10$m submitted to the following boundary conditions: (i) clamped, (ii) supported, (iii) on a rigid central support and (iv) totally free is used. It also presents $\lambda = \omega r_o^2 \cdot (\rho h/D)^{1/2}$, $\rho = 1.0$, $D = Eh^3/\{12(1-\nu^2)\}$, $E = 1365$ and $\nu = 0.3$. The results were based on a discretization of 12 QL16 elements (Figure 5).

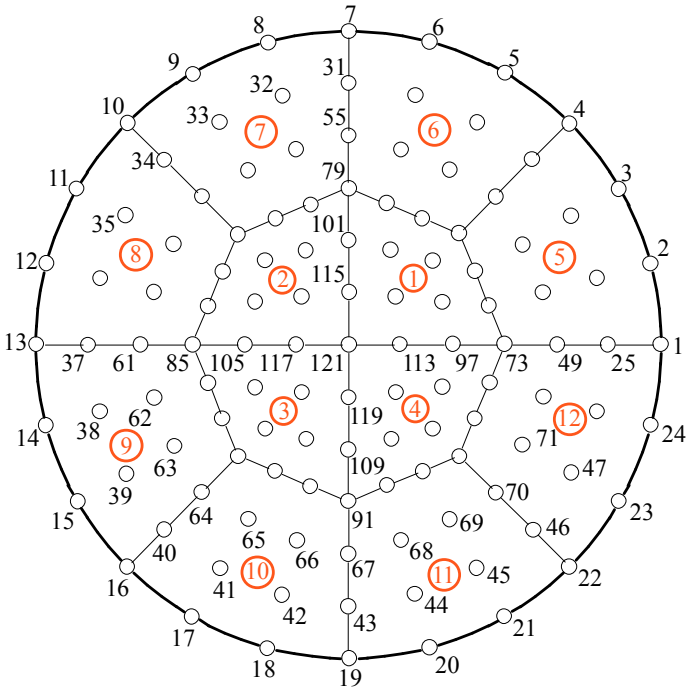

Figure 5 - Discretization of a Circular Plate with QL16 element.

Table 1 displays the values of λ_{mn}, where mn is the vibration mode rate. The Kirchhoff solution [2] for circular plates is adopted as an exact solution. The finite element employed provides excellent results for the fundamental frequencies of vibration of the circular plate, though the said element is "strained".

According to the analysis, for the first vibration mode the clamped boundary condition has a lower degree of numerical error than that of the support condition and the totally free condition, while for the second vibration mode the supported circular plate has the lowest degree of numerical error among the other two boundary conditions. For the third and fourth vibration modes, among the three types of support condition, the totally free circular plate is the one that provides the most accurate results through the analytical solution.

Table 1 - Comparative Study of Frequency Parameter, $\lambda = \omega r_o^2 \cdot (\rho h/D)^{1/2}$, to Circular Plates with Different Boundary Conditions, E = 1365; $\rho = 1$; $2r_o = 12$; h = 0.1.

BOUNDARY CONDITION	MODE (diameter and cycle modal)	QL16 (12 elements)	"EXACT" [2]	ERROR %
CAMPLED: $\nu = 0.3$ 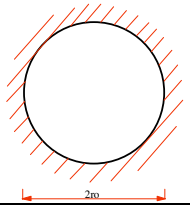	(0 , 0) (1 , 0) (2 , 0) (0 , 1)	10. 228 21. 316 35. 403 40. 405	10. 220 21. 260 34. 880 39. 771	-0. 078 -0. 263 -1. 499 -1. 594
SUPPORTED: $\nu = 0.3$ 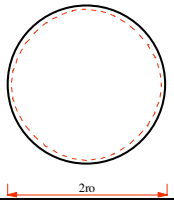	(0 , 0) (1 , 0) (2 , 0) (0 , 1)	4. 951 13. 921 25. 844 30. 296	4. 977 13. 940 25. 650 29. 760	0. 522 0. 136 -0. 756 -1. 801
CENTRAL SHAFT: $\nu = 1/3$ 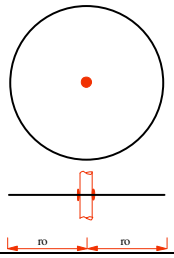	(0 , 0) (0 , 1) (0 , 2) (0 , 3) (0 , 4)	3. 808 21. 517 55. 243 132. 326 199. 879	3. 750 20. 900 61. 200 121. 000 200. 000	-1. 547 -2. 952 9. 734 -9. 360 0. 061
FREE: $\nu = 0.25$ 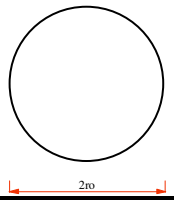	(2 , 0) (0 , 1) (3 , 0) (1 , 1)	5. 455 8. 800 12. 702 20. 173	5. 513 8. 892 12. 750 20. 410	1. 052 1. 035 0. 376 1. 161

VI. CONCLUSIONS AND PERSPECTIVES

The fact that we are dealing with a high-order element does not makes it inadequate for computational purposes (processing time in CPU), as the discretization can be done with rough meshes and still provide better results than other low-order elements that have been tested.

Generally, finite plate-bending elements based on the Reissner-Mindlin theory are not able to naturally create the slender plate condition, thus generating a *shear looking*

effect. With the QL16 element, this effect only occurs on exceptionally slender plates, whose dimension bears no physical sense, i.e., whose dimension has no practical application. This is another great advantage of the QL16 element over the low-order elements, which require techniques of imposed shearing or reduced integration to avoid the solution blocking effect.

For the cases analysed, the QL16 element proves to have excellent characteristics as it provides results whose error rate is lower than 5%.

VII. ACKNOWLEDGEMENTS

The authors would like to thank CNPq (National Council of Research) for scholarships and FAP/DF (Research Support Foundation - DF) for financial support for this work.

REFERENCES

[1] Timoshenko, S. and Woinowsky-Krieger, S., *Teoria de Placas y Laminas*, Ediciones Urmo, 1970, Spain.
[2] Szilard, R., *Theory and Analysis of Plates - Classical and Numerical Methods*, Prentice-Hall, Englewood Cliffs, 1974, New Jersey.
[3] Reissner, E., "The effect of transverse shear deformation on the bending of elastic plates," J.Appl.Mech., Vol.12, 1945, pp.69-76.
[4] Mindlin, R.D., "Influence of rotatory inertia and shear in flexural motions of isotropic elastic plates," *J.Appl.Mech.*, Vol.18, 1951, pp.31-38.
[5] Bathe, K.J. and Dvorkin, E., "A four-node plate bending element based on Mindlin/Reissner plate theory and a mixed interpolation," *Int.J.num.Meth.Engng.*, Vol.21, 1985, pp.367-383.
[6] Hinton, E. and Huang, H.C., "A family of quadrilateral Mindlin plate elements with substitute shear strain fields," *Computers & Strutures*, Vol.23, 1986, pp.409-431.
[7] Oñate, E., "Cálculo de estructuras por el método de elementos finitos - 2°Edición, análisis elástico lineal," *Centro Int. Métodos Num. Ingeniería*, Barcelona (1995).
[8] Zienkiewicz, O.C. and Taylor, R.L., *The Finite Element Method - Solid and Fluid Mechanics, Dynamics and Non-linearity*, McGraw-Will, Vol.2, 4°ed., 1991, Singapore.
[9] Silva, S.F., "Comportamento dinâmico de placas de Reissner-Mindlin utilizando o elemento finito quadrilátero lagrangeano de 16 nós," *Thesis of MSc, UnB-FT/EnC*, 1998, Brasil.
[10] Leissa, A.W., "The free vibration of retangular plates," *Comp. Meth. Appl. Mech. Eng.*, Vol. 55, 1986, pp.259-300.
[11] Dawe, D.J. and Roufaeil. O.L., "Rayleigh-Ritz vibration analysis of Mindlin plates," *J.Sound Vib.*, Vol.69, 1980, pp.345-359.
[12] Wilson, E.L. and Habibullah, A., "SAP90 - structural analysis users manual," *Computers & Structures*, 1992, Berkeley, California.

[13] Nildo Viana, J. *et.al.*, "Análise experimental dinâmica de placas mediamente espessa totalmente livre," *Relat. Interno de Ensaio n°30/97, UnB-FT/EnM-LTMD*, 1998, Brasil.